Graphene Sensors

International Edition: DOI: 10.1002/anie.201508300
German Edition: DOI: 10.1002/ange.201508300

A Graphene Fibriform Responsor for Sensing Heat, Humidity, and Mechanical Changes

*Fei Zhao, Yang Zhao, Huhu Cheng, and Liangti Qu**

Abstract: *Controllable and sensitive perception of environmental changes is essential for the development of smart material and device systems. Herein, a multi-stimuli sensitive responsor has been fabricated on the base of the established double-helix core-sheath graphene-based microfibers (GFs). By combining the tunable conductivity and mechanical robustness of GF coated with graphitic carbon nitride (GF@GCN), a fibriform smart environmental responsor (SER) is prepared by water-assisted GFs-twisting strategy, which can accordingly present conductive state-dependent current responses upon exposure to a variety of stimuli. More importantly, this SER exhibits high current response to small perturbations induced by temperature variations, mechanical interactions, and relative humidity changes, thereby achieving an environmental perceptibility. Based on this finding, a multi-functional respiratory monitor has been built under the stimuli of the human breath.*

Materials that can respond to external stimulations usher in a new era of materials science and engineering. Recently, great effort has been made to fabricate various smart systems, which can spontaneously respond to environmental changes such as force, temperature, humidity, and other stimuli.[1] Among them, graphene-based smart systems have been recognized as promising candidates to boost the high sensitivity and reliability similar to living organisms owing to the excellent electrical, thermal and mechanical properties of graphene, which thus was used for diverse applications ranging from sensors, detectors to actuators.[2] Ideally, the stimuli-responsive systems should be able to distinguish the external stimuli and respond to each of the specific chemical and/or physical variation. However, it is rather difficult for traditional single stimulus responsive systems to achieve this goal.

The boom of carbon-based fibers has presented potential applications for next-generation wearable electronics that are able to deform under bending, stretching, compressing, and twisting while still maintaining performance, reliability, and function. Potential applications include sensors for smart skins, photovoltaic wires for energy clothes, and fibriform supercapacitors for fabric batteries.[3] In this regard, graphene fiber (GF) fibriform electrodes have been attracting tremendous attention for years in the hopes of integrating unique properties such as light-weight, high-strength, and electrical and thermal conductivities of the individual nanoscale building blocks of graphene into the macroscopic ensembles.[4] Moreover, the chemical modification and structural modulation of GFs allows these functions to be incorporated into graphene-based electronic devices.

In this work, we present a multi-stimulus sensitive smart environmental responsor (SER) based on GFs, which can not only specifically distinguish the type of external stimuli, but also accurately detect the stimulation intensity. For this purpose, the GF was coated with a thin layer of graphitic carbon nitride (GCN) through electrochemical deposition (denoted as GF@GCN), and twisted with another GF to construct double-helix graphene fibers (DGF) with tunable conductive states (CSs). With a CS-dependent, stimuli-responsive current enhancement effect, the obtained DGFs present three types of sensing modes that specifically respond to temperature fluctuation, mechanical interaction, and humidity variation, respectively. This process offers an eco-friendly and low-cost fabrication of fibriform SER, which is able to selectively detect a slight temperature change ($\Delta T = 4\,^{\circ}C$), small force (0.05 N for press and 0.3 N for pull), and trace of moisture (relative humidity, RH = 3 %), with current responsive ratios of up to about 10^2 for a long-term test.

The GF@GCN was prepared by electrochemical electrolysis of a 0.5 mg mL^{-1} GCN aqueous suspension containing 1 M sulfuric acid (H_2SO_4) on GF at an applied potential of −0.6 V for 6 h (see Supporting Information for details). The obtained GF@GCN presented a core-sheath structure of the GF surrounded with a layer of GCN (Figure 1 a), which had an excellent flexibility (Figure 1 b) and a diameter of approximately 30 μm (Figure 1 c), comparable to the initial GFs (Supporting Information, Figure S1). Furthermore, the GF@GCN exhibited a relatively larger tensile strength than that of the initial GF (Supporting Information, Figure S2), indicating the deposition of GCN on GF does not impair its intrinsic mechanical properties. During the electrolysis process, GCN sheets (Supporting Information, Figures S3, S4) were deposited on the surface of GFs and self-assembled into a coating layer in accordance with the surface morphology of GFs (Figure 1 d). Moreover, the uniform decoration of GCN is demonstrated by the identical distribution of carbon and nitrogen elements along the whole fiber (Figure 1 e, f). The cross-section view shows an approximate 80 nm thick GCN layer without clear interface between GCN layer and the initial GF body (Figure 1 g,h), suggesting the compact contact of GCN with GF surface, which largely facilitates the

[*] F. Zhao, Dr. Y. Zhao, H. Cheng, Prof. L. Qu
Beijing Key Laboratory of
Photoelectronic/Electrophotonic Conversion Materials
Key Laboratory of Cluster Science, Ministry of Education
School of Chemistry, Beijing Institute of Technology
Beijing 100081 (P.R. China)
E-mail: lqu@bit.edu.cn

Supporting information for this article is available on the WWW under http://dx.doi.org/10.1002/anie.201508300.

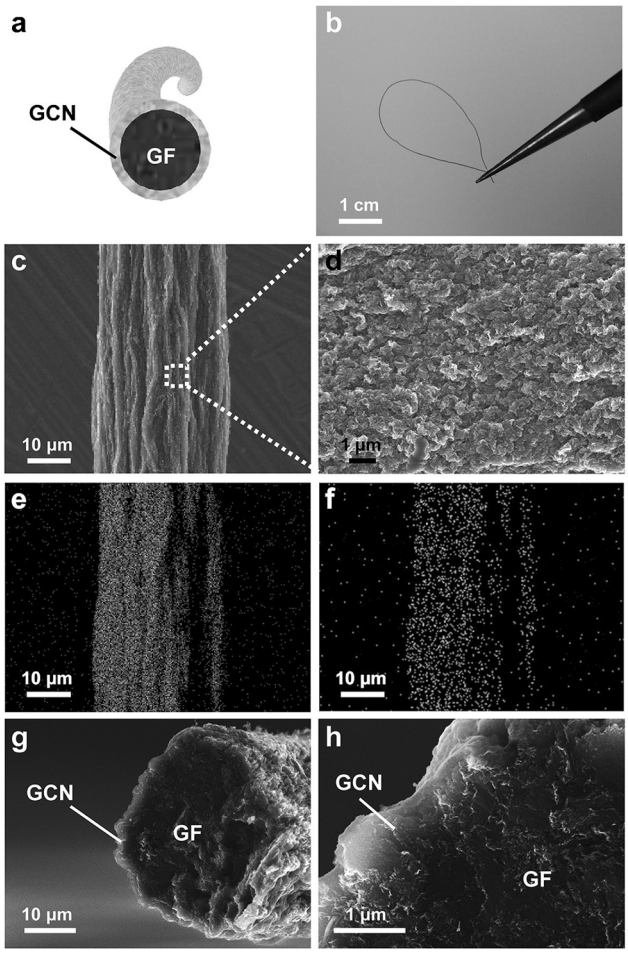

Figure 1. a) Illustration and b) photo of a deliberately distorted GF@GCN. c,d) SEM images of a GF@GCN and the enlarged surface view. e,f) The element mapping of C and N for a GF@GCN. g) Cross-section view of a GF@GCN showing the GF surrounding with a layer of GCN. h) The edge view of a GF@GCN.

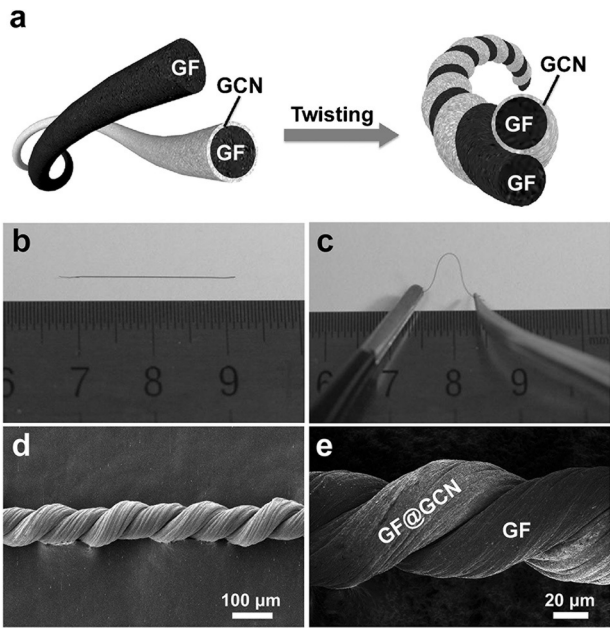

Figure 2. a) Illustration of DGF fabricated from intertwining GF@GCN and GF. b,c) Photos of a DGF in free and bending state. d,e) SEM images of the double-helix structure of GF@GCN and GF under different magnifications.

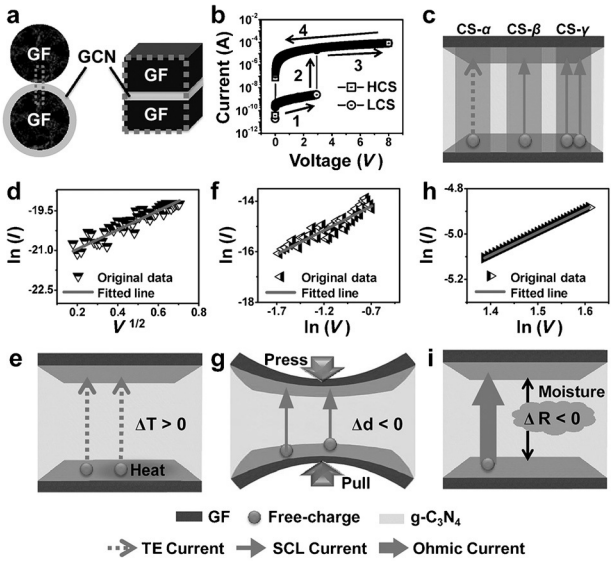

Figure 3. a) Illustration of the sandwich structure in the DGFs. b) *I*--*V* characteristics of the DGF with high conductive state (H-CS) and low conductive state (L-CS) under swept voltage along the arrows from 1 to 4. c) Diagram of basic thermionic emission (TE) current and space charge limited (SCL) current of CS α, β, and γ, respectively. d) Experimental data and fitted lines of TE current and e) corresponding illustration of heat-enhanced charge transport in CS-α. f) Experimental data and fitted lines of SCL current and g) corresponding illustration of force-enhanced charge transport in CS-β. h) Experimental data and fitted lines of ohmic current and i) corresponding illustration of moisture-enhanced charge transport in CS-γ.

dielectric effect for the transfer of charges to form stable microcurrents under applied voltage (Supporting Information, Figure S5).

Based on the ideal conductivity of GF, dielectricity of the GCN layer, and the high flexibility of GF@GCN, we built the DGF by intertwining a GF@GCN with a GF (Figure 2a). The obtained DGF maintains good fiber shape with excellent flexibility and mechanical strength (Figure 2b,c; Supporting Information, Figure S6). The double-helix structure of GF@GCN and GF was uniform and tight (Figure 2d), which provided effective electron transfer for the injection of charges to form stable currents under applied voltage.[3c] Moreover, the enlarged view of the twisted fibers presents different brightness of GF@GCN and GF under electron irradiation (Figure 2e), owing to the different conductivity of GCN and graphene.

Based on our previous work, the dielectricity of the thin GCN layer between electrodes could be adjusted by applied voltage.[5] The contact interface of the two fibers in DGF can be regarded as a sandwiched graphene/GCN/graphene structure (Figure 3a), where the graphene serves as electrodes and the GCN functions as a thin dielectric layer. Thus, the DGF can also provide different conductive states (CSs) under the control of applied voltages. As shown in Figure 3b, the CS of DGF was controlled by a pre-treatment of swept voltages

ranging from 0 to 8 V. Initially, the as-prepared DGF showed a low conductive state (L-CS), and the current increased progressively with the voltage increase (Figure 3b, arrow 1). When the applied voltage exceeded a switching threshold voltage of about 3.1 V, an abrupt current increase occurred (Figure 3b, arrow 2), indicating a transition from the low-current state to the high-conductive state (H-CS) caused by the dielectric loss of the dielectric layer. Once this transition was achieved, the CS was stably retained (Figure 3b, arrows 3,4; Supporting Information, Figure S7) until the negative voltage was applied.

To understand this CS transform, the analysis of experimental *I*--*V* data from specific voltage ranges showed that the current of L-CS under applied voltages in range of 0 to 0.5 V (denote as CS-α) was dominated by thermionic emission (TE) current (Supporting Information, Figure S7).[5] Similarly, the analysis in Figure S8 (Supporting Information) indicated that the current of H-CS under applied voltages in range of 0 to 0.5 V and 4 to 5 V were supported by space-charge-limited (SCL) currents and electric field-enhanced SCL currents, which were accordingly denoted as CS-β and CS-γ, respectively (Figure 3c).[5] Notably, the mathematic expressions of TE current and SCL current (Supporting Information, Figures S8,S9 and Equations S1,S3) revealed dependencies of the current intensity and environmental parameter (for example, temperature for CS-α), implying a CS-dependent current response to environmental variations.

Figure 3d shows the *I*--*V* characteristic of DGF in CS-α with a $\Delta T = 4\,^{\circ}C$, where the experimental data of ln (*I*) and $V^{1/2}$ could be fitted to a straight line upon Equation S1, suggesting that the heat-enhanced charge transport in CS-α was also dominated by the TE current. Such a current is severely limited by the lack of available free charges. Therefore, the current enhancement can be achieved by a heating process that can activate extra free charges, where force and moisture can rarely enhance the current, presenting a voltaic response to temperature change (Figure 3e).[6] Moreover, the *I*--*V* characteristic of the DGF in CS-β with pressing force of 0.05 N was observed in the plot of ln (*I*) versus ln (*V*) based on Equation S3 (Figure 3f), indicating SCL current dominated the charge transport process, and more importantly, revealing a negative dependency between current and electrode spacing value (*d*; Figure 3g.[7] This decrease of *d*, combining the press-induced increase of contact area between GFs (Supporting Information, Figure S10) and leading to more obvious current enhancement than moisture and heat, enabled a voltaic response to the force. Interestingly, when the DGF was exposed to moist air, Figure 3h displayed the plot of ln (*I*) versus ln (*V*) and the fitted line with a slope of 1.06, implying an ohmic current of DGF in CS-γ. Normally, in view of the strong electronic dielectricity, GCN coating layer is scarcely possible to support the ohmic current, even if the ionic polarization assisted current increase can be further enlarged by moisture.[8] However, under a ultra-strong electric field (ca. $6\times10^{7}\,V\,m^{-1}$), the water molecular adsorbing on the surface of GCN nanosheets were able to create extra conductive channels to achieve an ohmic surface current beyond the intrinsic SCL current. Therefore, despite the weak current enhancement of forces, the DGF exhibited extremely enlarged currents triggered by moisture (Figure 3i), thus providing moisture sensitivity. These results revealed that the current responses were caused by the CS-dependent dielectric loss of the dielectric layer, which presented various sensitivities toward external stimuli, and therefore the controllable sensing of environmental changes.

To demonstrate the controllable sensitivities toward environmental changes mentioned above, a DGF-based fibriform SER (DGF-SER) was exposed to heat, force loads, and moist air (Figure 4a; Supporting Information, Figures S11–

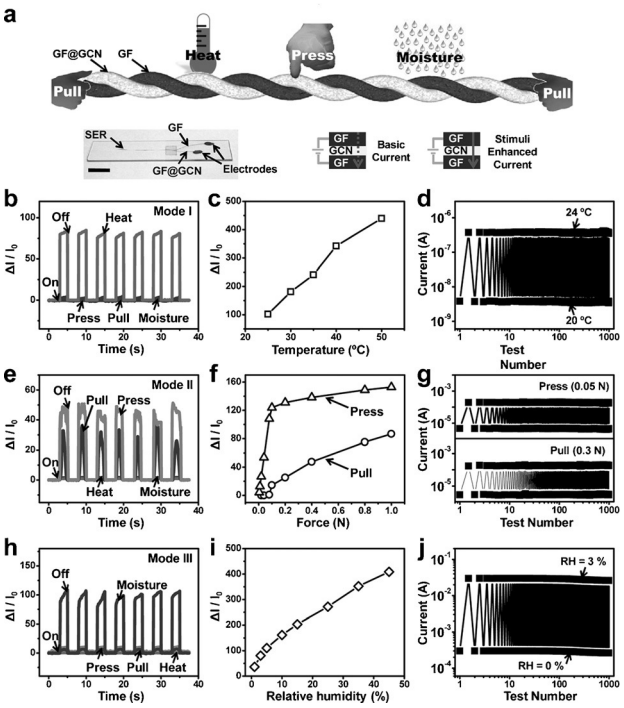

Figure 4. a) Illustration of the heat, moisture, horizontal pull, and vertical press force loaded on the DGF. Inset: Photograph of SER device and diagram of its operation mechanism. Scale bar = 1 cm. b) Current response, c) quantitative relationship of $\Delta I/I_0$ versus temperature, and d) stability test of the SER for the various applied stimuli in Mode I (thermo-sensitive mode). e) Current response, f) quantitative relationship of $\Delta I/I_0$ versus Force, and g) stability test of the SER for the various applied stimuli in Mode II (force-sensitive mode). h) Current response, i) quantitative relationship of $\Delta I/I_0$ versus humidity, and j) stability test of the SER for the various applied stimuli in Mode III (moisture-sensitive mode). The thermal, mechanical, and moisture responses in b, d, e, g, h, and j correspond to the temperature variation of 4 °C, 0.05 N for vertical press, 0.3 N for horizontal pull and 3% for RH, respectively. The applied voltages of the SER are 0.3 V for Mode I, Mode II, and 5 V for Mode III. ΔI and I_0 represent the variation of current and initial current, respectively.

S13). The specific current response (current change/initial current, $\Delta I/I_0$) to temperature variation (ΔT) was measured with $\Delta T = 4\,^{\circ}C$ under applied voltage of 0.3 V when DGF was in L-CS, where the heat caused $\Delta I/I_0$ was approximately 80 (Figure 4b) and the signals of other stimuli (moisture and force) were negligible (Supporting Information, Figure S14), showing a temperature-sensitive mode (denoted as Mode I) of the DGF-SER. The temperature-sensitivity of Mode I,

which was defined as $\Delta I/I_0$ caused by ΔI of 1 °C on average, was evaluated by the quantitative relationship of $\Delta I/I_0$ versus ΔT (Figure 4c), where a high sensitivity of approximately 16 per °C was seen in the temperature range of 20 to 50 °C (Supporting Information, Figure S15), indicating that the DGF-SER was able to be used as a temperature sensor. The durability and stability of the Mode I were investigated through repeated heat–cold cycling tests between 20 and 24 °C. As shown in Figure 4d, the output signals of the DGF-SER were stably maintained without any remarkable degradation despite 1000 times cycling tests, indicating a highly reliable detection of SER for temperature variation.

Figure 4e–g shows the sensing behavior of DGF-SER in a force-sensitive mode (Mode II). Owing to the double-helix structure of the DGF-SER, the relatively strong horizontal pull, which is analogous with the vertical press, can induce a stress between GFs, and hence both press and pull could be detected in Mode II. The $\Delta I/I_0$ of DGF-SER under vertical press of 0.05 N and horizontal pull of 0.3 N were tested to be about 50 and 35 under applied voltage of 0.3 V when the DGF was regulated to H-CS, respectively (Figure 4e), while the feedback to heat and moisture tests were unobservable (Supporting Information, Figure S16). Moreover, the quantitative relationship of force versus $\Delta I/I_0$ showed linear correlations in different regions (Figure 4f), suggesting the ultra-high force-sensitivity ($\Delta I/I_0$ caused by 1 N on average) of about 1400 per N in the low pressure range of less than 0.1 N, high force-sensitivity of about 27 per N for press and 77 per N for pull in the range of 0.1 to 1 N (Supporting Information, Figure S17). Although the DGF-SER presented impressive force-sensitivity, the stable $\Delta I/I_0$ of Mode II were maintained after 1000 testing cycles (Figure 4g). These results demonstrated that the SER was able to sever as a high-performance force sensor.

On the other hand, as an ideal SER, the DGF can further function as a moisture-responsor under applied voltage of 5 V (Mode III) based on its H-CS, which presented a $\Delta I/I_0$ of ca. 140 (Figure 4h) with ΔRH of 3%, eliminating the interruptions of other stimuli (Supporting Information, Figure S18). The moisture-sensitivity ($\Delta I/I_0$ caused by ΔRH of 1% on average) was 23 per 1% when the RH was less than 5%, while a slightly-lower moisture-sensitivity of 7 per 1% was observed upon environmental *RH* ranging from 5 to 45% (Figure 4i; Supporting Information, Figure S19). Furthermore, the duration test with *RH* between 0% and 3% indicated a reliable humidity-response of DGF-SER after 1000 cycles (Figure 4j), Therefore, the DGF-SER could be considered as a high performance humidity sensor. More importantly, the sensitivity and flexibility (Supporting Information, Figure S20) of this DGF-SER for each stimulus was higher than or comparable with that of other single-selective sensors.[9]

To explore the application of the DGF-SER, a prototype of multifunctional body condition monitor has been developed. For instance, by simulating the vibrissa of terrestrial animals, a bionic nasal cavity was fabricated by DGF-SER and a commercial polyethylene (PE) tube to detect the breath of human (Figure 5a–c). The respiratory temperature, frequency, and moisture content can be monitored by calculating the peak value and counting the number of exhalation (or

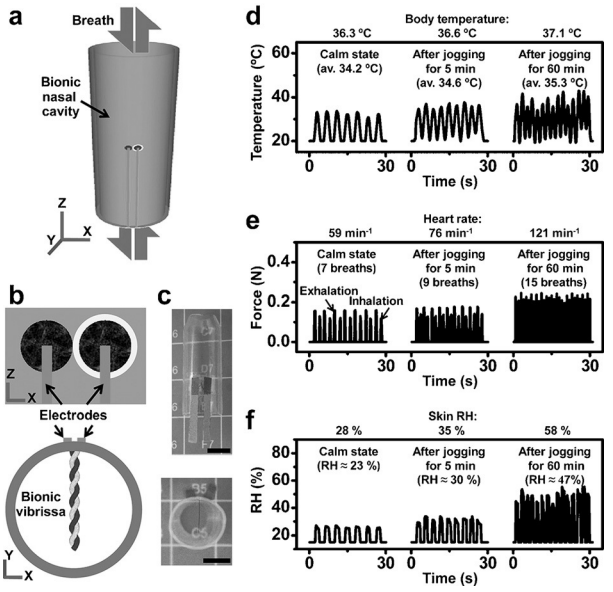

Figure 5. a) Illustration of the bionic nasal cavity body condition monitor fabricated by DGF-SER and commercial PE tube with b) side view and sectional view. c) Side view and sectional view photographs of DGF-SER-based body condition monitor. Scale bar = 2 cm. d) Monitoring of human respiratory temperature, frequency and RH of relating to body temperature, heart rate, and skin RH upon calm state, light exercise, and strenuous exercise, respectively.

inhalation) pulses of the feedback signals upon Mode I, II, and III of DGF-SER, respectively. As shown in Figure 5d,e, before jogging, the calm breathing of a healthy man was warm (34.2 °C), steady (14 times per minute) and slightly moist (with RH of ca. 23%), corresponding a body temperature of 36.3 °C, a heart rate of 59 times per minute and skin RH of about 28%. After jogging for 5 min, the breathing was accelerated to 18 times per minute with incidental temperature of 34.6 °C and RH of 30%, accompanied by a body temperature of 36.6 °C, a heart rate of 80 beats per minute and skin RH of 35%. Moreover, when the jogging time was extended to 60 min, the signals representing rapid breathing (30 times per minute) with damp and warm exhalation (RH of ca. 47% and 35.3 °C) were observed, and the body temperature (37.1 °C), heart rate (121 beats per minute) and skin RH (ca. 58%) were increased. These results experimentally revealed that the close relevance of respiratory temperature versus body temperature, respiratory frequency versus heart rate, and respiratory RH versus skin RH with coefficiencies of 1.4, 4.1, and 1.2 for different body conditions (Supporting Information, Figure S21), respectively. This simple demonstration revealed the great potential of DGF-SER for monitoring body condition towards clinical diagnosis.

In summary, a unique graphene-based fibriform SER composed of a double helix of two GFs has been newly designed and fabricated, in which one GF is decorated with a thin coating of modified GCN as a functional layer. The GCN coating enabled the DGF-SER to provide three stable CSs, which are achieved by preloading voltages, for the selective detection of small temperature fluctuations, mechanical interactions, and humidity variations with high

reliability. More importantly, these controllable responses are reliable, retaining the high sensitivity and excellent repeatability of stimuli-responsive effect over time, as well as possessing the impressive ability to recognize the type of external stimuli. On the basis of the CS-dependent detection of environment, a multifunctional human body monitor has been constructed by using DGF-SER as the vibrissa in a simulated nasal cavity to monitor human breath. This work aims to advance the concept of a flexible, highly-sensitive fibriform SER with integrated functions of environmental response, identity, and monitoring. We anticipate that the DGF-SER will be a promising candidate for applications in future smart systems by combining advanced electronic techniques.

Acknowledgements

This work was supported by NSFC (No. 21325415, 21174019), National Basic Research Program of China (2011CB013000), Beijing Natural Science Foundation (2152028).

Keywords: environmental sensors · fibers · graphene · graphitic carbon nitride · materials science

How to cite: *Angew. Chem. Int. Ed.* **2015**, *54*, 14951 – 14955
Angew. Chem. **2015**, *127*, 15164 – 15168

[1] a) D. Kang, P. V. Pikhitsa, Y. W. Choi, C. Lee, S. S. Shin, L. Piao, B. Park, K. Y. Suh, T. i. Kim, M. Choi, *Nature* **2014**, *516*, 222 – 226; b) C. Dagdeviren, Y. Shi, P. Joe, R. Ghaffari, G. Balooch, K. Usgaonkar, O. Gur, P. L. Tran, J. R. Crosby, M. Meyer, *Nat. Mater.* **2015**, *14*, 728 – 736; c) X. Chen, D. Goodnight, Z. Gao, A. H. Cavusoglu, N. Sabharwal, M. DeLay, A. Driks, O. Sahin, *Nat. Commun.* **2015**, *6*, DOI: 10.1038/ncomms8346; d) G. Zabow, S. Dodd, A. Koretsky, *Nature* **2015**, *520*, 73 – 77.

[2] a) J. Zhang, L. Song, Z. Zhang, N. Chen, L. Qu, *Small* **2014**, *10*, 2151 – 2164; b) P. Kim, C. M. Lieber, *Science* **1999**, *286*, 2148 – 2150; c) A. Fennimore, T. Yuzvinsky, W. Q. Han, M. Fuhrer, J. Cumings, A. Zettl, *Nature* **2003**, *424*, 408 – 410; d) S. V. Ahir, E. M. Terentjev, *Nat. Mater.* **2005**, *4*, 491 – 495; e) J. D. Madden, *Science* **2006**, *311*, 1559 – 1560.

[3] a) H. B. Yao, J. Ge, C. F. Wang, X. Wang, W. Hu, Z. J. Zheng, Y. Ni, S. H. Yu, *Adv. Mater.* **2013**, *25*, 6692 – 6698; b) Z. Yang, H. Sun, T. Chen, L. Qiu, Y. Luo, H. Peng, *Angew. Chem. Int. Ed.* **2013**, *52*, 7545 – 7548; *Angew. Chem.* **2013**, *125*, 7693 – 7696; c) Y. Meng, Y. Zhao, C. Hu, H. Cheng, Y. Hu, Z. Zhang, G. Shi, L. Qu, *Adv. Mater.* **2013**, *25*, 2326 – 2331; d) L. Kou, T. Huang, B. Zheng, Y. Han, X. Zhao, K. Gopalsamy, H. Sun, C. Gao, *Nat. Commun.* **2014**, *5*, 3754; e) L. Liu, Y. Yu, C. Yan, K. Li, Z. Zheng, *Nat. Commun.* **2015**, *6*, 7260.

[4] a) Z. Dong, C. Jiang, H. Cheng, Y. Zhao, G. Shi, L. Jiang, L. Qu, *Adv. Mater.* **2012**, *24*, 1856 – 1861; b) H. Cheng, J. Liu, Y. Zhao, C. Hu, Z. Zhang, N. Chen, L. Jiang, L. Qu, *Angew. Chem. Int. Ed.* **2013**, *52*, 10482 – 10486; *Angew. Chem.* **2013**, *125*, 10676 – 10680; c) H. Cheng, Y. Hu, F. Zhao, Z. Dong, Y. Wang, N. Chen, Z. Zhang, L. Qu, *Adv. Mater.* **2014**, *26*, 2909 – 2913.

[5] F. Zhao, H. Cheng, Y. Hu, L. Song, Z. Zhang, L. Jiang, L. Qu, *Sci. Rep.* **2014**, *4*, 5882.

[6] a) G. Sun, J. Liu, X. Zhang, X. Wang, H. Li, Y. Yu, W. Huang, H. Zhang, P. Chen, *Angew. Chem. Int. Ed.* **2014**, *53*, 12576 – 12580; *Angew. Chem.* **2014**, *126*, 12784 – 12788; b) J. Liu, Z. Yin, X. Cao, F. Zhao, L. Wang, W. Huang, H. Zhang, *Adv. Mater.* **2013**, *25*, 233 – 238.

[7] Z. Q. Lin, J. Liang, P. J. Sun, F. Liu, Y. Y. Tay, M. D. Yi, K. Peng, X. H. Xia, L. H. Xie, X. H. Zhou, *Adv. Mater.* **2013**, *25*, 3664 – 3669.

[8] U. Mogera, A. A. Sagade, S. J. George, G. U. Kulkarni, *Sci. Rep.* **2014**, *4*, 4103.

[9] a) X. Ren, P. K. Chan, J. Lu, B. Huang, D. C. Leung, *Adv. Mater.* **2013**, *25*, 1291 – 1295; b) Y. Chen, B. Lu, Y. Chen, X. Feng, *Sci. Rep.* **2015**, *5*, 11505; c) L. Viry, A. Levi, M. Totaro, A. Mondini, V. Mattoli, B. Mazzolai, L. Beccai, *Adv. Mater.* **2014**, *26*, 2659 – 2664; d) Y. S. Zhou, R. Hinchet, Y. Yang, G. Ardila, R. Songmuang, F. Zhang, Y. Zhang, W. Han, K. Pradel, L. Montès, *Adv. Mater.* **2013**, *25*, 883 – 888; e) H. Bi, K. Yin, X. Xie, J. Ji, S. Wan, L. Sun, M. Terrones, M. S. Dresselhaus, *Sci. Rep.* **2013**, *3*, 2714; f) W. Xuan, M. He, N. Meng, X. He, W. Wang, J. Chen, T. Shi, T. Hasan, Z. Xu, Y. Xu, *Sci. Rep.* **2014**, *4*, 7206.

Received: September 5, 2015
Published online: October 12, 2015

